



**Efficiencies of Removing Dust
on
Acrylic Plastic Surfaces
by
Non-agitated De-ionized Water**

**by
Eric Kong
Engineering Assistant
Sudbury Neutrino Observatory Project
Lawrence Berkeley Laboratory
Berkeley, California
11 January, 1993**

SNO-STR-92-083

Efficiencies of Removing Dust on Acrylic Plastic Surfaces by Non-agitated De-ionized Water

by
Eric Kong

Abstract

To find out how much dust can be removed from the acrylic vessel's outer surface when slowly filling the SNO cavity with water, we conducted several experiments, which simulate anticipated conditions. This report describes the five experiments we conducted and summarizes the results. De-ionized water was used for cleaning the acrylic plastic samples. These samples were prepared in two sizes, 0.25"x2"x3" and 0.25"x4"x6", and different amounts of dust were blown on their surfaces. They were then immersed in de-ionized water. The amount of dust removed by the water was determined by x-ray fluorescence analysis of adhesive tapes applied to the sample surfaces before and after immersion. Since the dust removal efficiency might depend on the amount of dust on the surface, how fast the dusty acrylic plastic sample was inserted into water, or the water level rising rate, several different experiments were made. In seven out of eight measurements, the mass fraction of the dust removed varied from about 70% to 98%.

Table of Contents

	<u>Pages</u>
Abstract	i
1.0 Introduction	1
2.0 Experiment I	
2.1 Preparation and Procedure	1-3
2.2 Results	3-4
3.0 Experiment II	
3.1 Preparation and Procedure	5
3.2 Results	6
4.0 Experiments III and IV	
4.1 Preparation and Procedure	6-7
4.2 Results	7-8
5.0 Experiment V	
5.1 Preparation and Procedure	8-10
5.2 Results	10
6.0 Summary	10-11
Appendix	12

List of Figures

Figure

1. The two dusty acrylic plastic samples are placed into two 400 mL beakers, one with de-ionized water.	2
2. Filtering process.	3
3. A dusty acrylic plastic sample is put into de-ionized water in experiment II.	5
4. Adding de-ionized water into the beaker that contains a dusty acrylic plastic sample.	7
5. Using a siphon to add and empty the beaker that contains a dusty acrylic plastic sample.	9
6. Efficiency of dust removed by water versus different amounts of dust on acrylic plastic surfaces.	11

List of Tables

Table

1. XRF and optical counting results of tape lift tests on 2"x 3" samples in experiment I.	4
2. XRF results of tape lift tests on a 4"x 6" sample in experiment II.	6
3. XRF results of tape lift tests on 4"x 6" samples in both experiments III and IV.	8
4. XRF results of tape lift tests on 4"x 6" samples in experiment V.	10

Efficiencies of Removing Dust on Acrylic Plastic Surfaces by Non-agitated De-ionized Water

by
Eric Kong

1.0 Introduction

At the SNO site, water will be slowly filling the cavity (outside and inside the acrylic vessel) and circulated through a filter and back to the cavity. Because the water is in an almost stable condition, we need to know if the dust on the acrylic vessel's outer surface will be removed by the water. This situation (static water) is to be distinguished from an active cleaning process (e.g., rinsing) in which the rinse water is moving rapidly and may remove dust by mechanical action as well as by wetting. Therefore, we conducted experiments simulating the fill process to measure the amount of dust removed. This report describes the results we obtained for several experiments on the removal of mine dust from the acrylic plastic surfaces by nearly static de-ionized water.

2.0 Experiment I

2.1 Preparation and Procedure

In the first experiment, we prepared two pieces of 2"x3" samples (acrylic plastics 1 and 2) by washing them with soap and de-ionized water and drying them in a clean room. These sample surfaces were maintained as clean as possible. After they were cleaned and hung inside the glove-box, we blew mine dust on the sample surfaces. After the dust had completely settled on the sample surfaces, we took them off the hanger inside the glove-box, immediately placed them into two 400 mL beakers (one was empty and the other was filled with 325 mL de-ionized water), and covered them to prevent dust entering from outside -- see Figure 1. Because the sample was put into the water slowly (in about five seconds), the water was non-agitated.

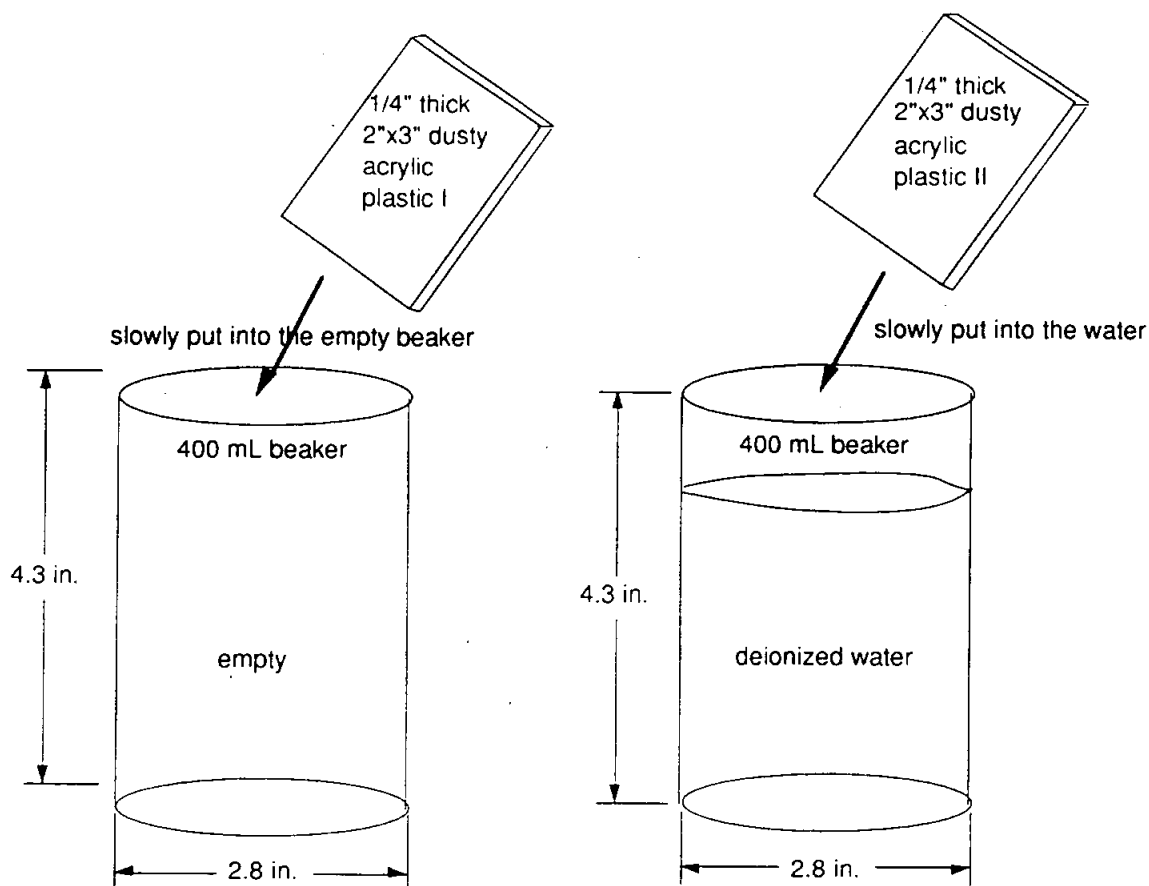


Figure 1. The two dusty acrylic plastic samples are placed into two 400 mL beakers, one with de-ionized water.

We then brought them to the clean room, which is in another building. We first did tape-lift tests on both surfaces of the first sample, acrylic plastic 1, after it was slowly taken out from the empty beaker. After the second sample had been in the 325 mL de-ionized water for about 30 minutes, we took about five seconds to lift the sample out of the water and then placed it in the empty beaker and let it dry. A special filtering syringe sucked the 325 mL water out of the beaker and pumped the water through a 4.15 cm diameter teflon filter, which was kept inside a circular case attached to the syringe exit (see Figure 2). The teflon filter was used to collect most of the dust suspended in water.

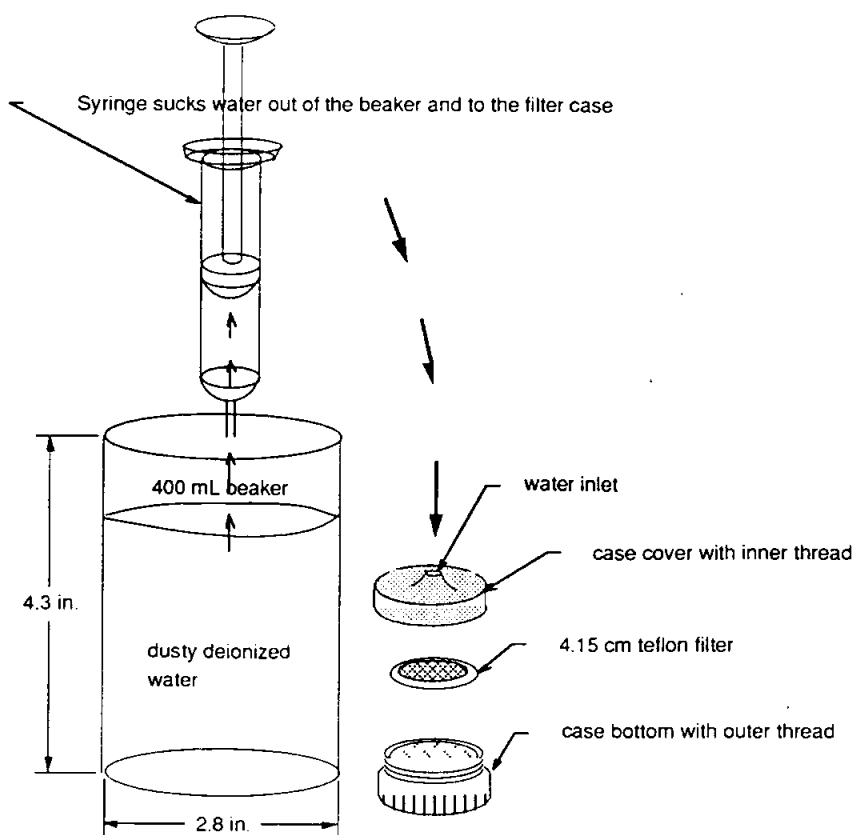


Figure 2. Filtering process

After the second sample was dry, we performed the tape-lift tests on both surfaces. All these tapes and filters (including a background tape) were sent for x-ray fluorescence analysis (XRF). In addition, optical counting was done on the surfaces of acrylic plastic samples 1 and II.

2.2 Results

The acrylic tape-lift test results, include XRF and optical counting, are listed in Table 1. In summary, dust was deposited on samples 1 and 2 at the same time (i.e. with the same dust blow). Sample 1 was used to determine the amount of dust deposited by measuring the amount of dust deposited on each side. We assumed the same amount of dust would be deposited on sample 2. Sample 2 was immersed in de-ionized water and the amount of dust remaining on it was measured. The different values obtained on the two sides of sample 1 (2.75 and 1.63 $\mu\text{g}/\text{cm}^2$) suggest that the assumption of uniform deposition was valid to within a factor of two. Because sample 2 was kept in de-ionized water when being transferred to the clean room, we characterize the immersion as lightly agitated. Results for dust suspended in the water and collected on the teflon filters are not included in this report and will be discussed in another report.

	Dust amount on the #369 Mylar tape ($\mu\text{g}/\text{cm}^2$)		Optical Counting on 2"x3" Acrylic plastic dusty area
	Before immersion	After immersion	
Acrylic Plastic 1 (Side A)	2.75 \pm 0.12	N/A Never immersed	$N=473,387 \cdot D^{-2.146}$ (N is the number/cm ² & D is in μm)
Acrylic Plastic 1 (Side B)	1.63 \pm 0.12	N/A Never immersed	$N=296,202 \cdot D^{-2.322}$
Acrylic Plastic 2 (Side A)	N/A	0.72 \pm 0.10	$N= 25,878 \cdot D^{-1.817}$
Acrylic Plastic 2 (Side B)	N/A	0.17 \pm 0.08	$N(D \geq 5\mu\text{m})=202$ particles

Table 1. XRF and optical counting results of tape-lift tests on 2"x 3" samples in experiment I.

The above table indicates that a significant amount of dust is removed from the acrylic plastic surfaces by the lightly agitated water. The optical counting results corresponding to the samples are consistent with the dust level on the sample surface indicated by the XRF done on the lifted tapes. Comparing the *before* and *after* immersion tape-lift test results in both experiments, we can then obtain the efficiency of removing dust with de-ionized water by using the following formula.

$$\% \text{ dust removal} = \frac{(\text{Before immersion}) - (\text{After immersion})}{\text{Before immersion dust amount}} \times 100$$

The average amount of dust for both sides of sample I is 2.2 \pm 0.6 $\mu\text{g}/\text{cm}^2$, where we have included an estimate of systematic errors. The average amount of dust left on sample II after immersion is 0.45 \pm 0.3 $\mu\text{g}/\text{cm}^2$, also including an estimate of systematic errors. Therefore, the average dust removal is about 80 percent.

There were two problems with this experiment that we felt could be minimized by changing procedure. The first problem was that the surface area of the sample was small compared to the surface area of the container, which made the measurements of the dust in the water less reliable. The second problem was the non-uniformity of the dust deposition on different sample surfaces. Therefore, we increased the sample size in the second experiment and performed the tape-lift test on the same sample *before* and *after* immersion.

3.0 Experiment II

3.1 Preparation and Procedure

The second experiment was performed with one piece of 4"x 6" acrylic plastic sample. It was rinsed with de-ionized water and dried in a clean room. (Because the sample was covered with protective paper and found to be clean, it was not washed with soap.) After it was cleaned and hung inside the glove-box, we blew mine dust on the sample surfaces (two sides). After dust had completely settled on the sample surfaces, we took this sample off the hanger inside the glove-box and put it into a 2000 mL beaker. We then covered the beaker with plastic wrap to prevent dust entering from outside. We brought the beaker with sample to the clean room and performed tape-lift tests with the #369 mylar tape. We first did the tape-lift tests on both surfaces of the sample from the beaker. For each sample, we used the same tape, repeatedly pressing and lifting it at four different places, trying to get an average distribution because of the non-uniform dust deposition on the acrylic plastic surface. Then, this sample was slowly (in about five seconds) put into a 6" x 8" tray with 325 mL de-ionized water (see Figure 3).

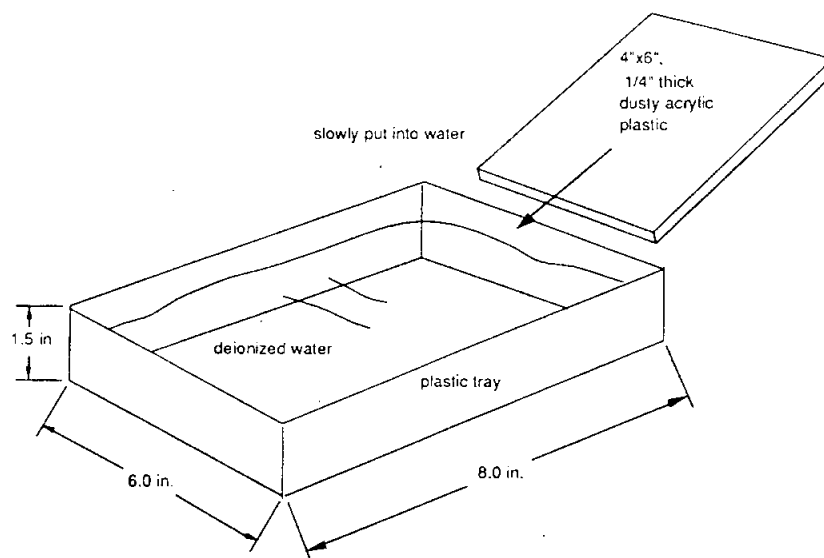


Figure 3. A dusty acrylic plastic sample is put into de-ionized water in experiment II

About half an hour later, we slowly took the sample out of the tray and back to the beaker. We sucked the 325 mL water out of the beaker and pumped the water through a 4.15 cm diameter teflon filter, which was kept inside a circular case attached to the syringe exit. After the acrylic sample was dry, we did the tape-lift tests on both surfaces of the sample, again pressing and lifting a tape at four different places (not previously sampled) on the sample surfaces. All these tapes (including a background tape) were sent for x-ray fluorescence analysis.

3.2 Results

Table 2 shows the results of the second experiment. Because water was involved in the immersion process only after sample had been transferred to the clean room and slowly immersed into water, we characterize this immersion as non-agitated.

	Dust amount on the #369 Mylar tape ($\mu\text{g}/\text{cm}^2$)	
	Before immersion	After immersion
Acrylic Plastic sample	33.3 \pm 1.3	5.5 \pm 0.2

Table 2. XRF results of tape-lift tests on a 4"x 6" sample in experiment II.

The above table indicates that a significant amount of dust was removed by the water from the sample surface. Comparing the *before* and *after* immersion tape-lift results, we can then obtain the efficiency of removing dust with de-ionized water by using the formula mentioned in experiment I. A dust removal of about 83 percent is indicated by this second experiment.

4.0 Experiments III and IV

4.1 Preparation and Procedure

The third and fourth experiments were each performed with two 4"x 6" acrylic plastic samples. The only difference between these experiments is that experiment IV had smaller amount of dust blown on the sample surfaces than experiment III. Both acrylic plastic samples were rinsed with de-ionized water and dried in a clean room. We blew mine dust on the cleaned samples. After dust had completely settled in the glove-box, we took the samples off the hanger and put them into two 2000 mL beakers. We then covered the beakers with plastic wrap to prevent dust entering from outside. We brought them to the clean room and performed tape-lift tests with the #369 mylar tape. We first did the tape-lift tests on both surfaces of all the samples. For each sample, we used the same tape, repeatedly pressing and lifting it at four different places on both surfaces, trying to get an average distribution because of the non-uniform dust deposition on the acrylic plastic surface. Each of the samples was slowly put back into the beaker. Then, de-ionized water was added into the beaker with volume rate of 3.5 mL per second until 2000 mL water was in the beaker and, after about 9 minutes, had covered the entire acrylic plastic sample. Figure 4 shows this water filling process.

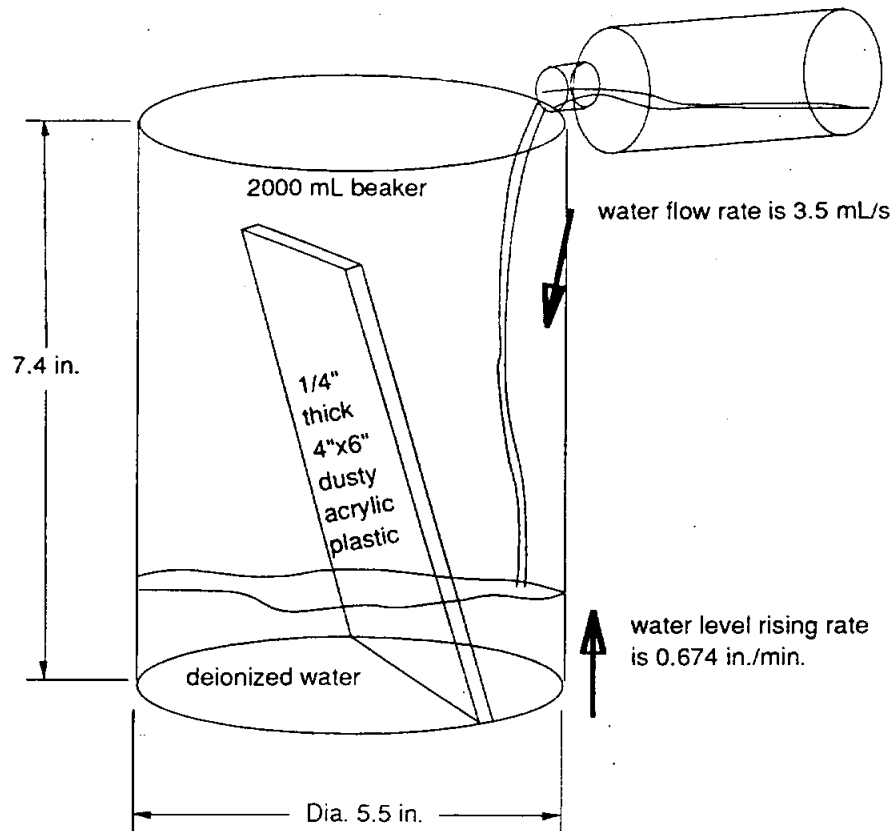


Figure 4. Adding de-ionized water into the beaker that contains a dusty acrylic plastic sample.

The figure shows that the water level rising rate is 0.674 in/min in our experiments, which is 32 times faster than the anticipated rate (0.021 in/min)^[1] in the cavity. If we were to simulate the exact water filling rate, it would have taken six hours to fill the beaker with 2000 mL. Water level rising rate of 0.674 in/min was chosen.

After the acrylic plastic samples stayed in the deionized water for 30 minutes, we slowly (about five seconds) took them out of the beakers. As soon as we emptied the beakers, we put the samples back to the beakers until the samples were dry. After the two samples were dry, we did the tape-lift tests on both surfaces of each sample, again pressing and lifting a tape at four different (not previously sampled) places on the sample surfaces. All these tapes (including a background tape) were sent for x-ray fluorescence analysis.

4.2 Results

Table 3 shows the x-ray results of both experiments III and IV.

[1] P.J. Zwart & J.P. Van Doormaal, "Sudbury Neutrino Observatory Light Water Flow Modeling," ASC Report # 90-1022-1, pp. 2-4, December 1990. *see appendix.

	Dust amount on the #369 Mylar tape ($\mu\text{g}/\text{cm}^2$)		Percentage of dust removed (%)
	Before immersion	After immersion	
Acrylic Plastic 1 (experiment III)	28.8 \pm 0.2	8.4 \pm 0.1	71 \pm 1
Acrylic Plastic 2 (experiment III)	0.98 \pm 0.03	0.82 \pm 0.03	16 \pm ₅ ⁶
Acrylic Plastic 1 (experiment IV)	4.5 \pm 0.1	0.60 \pm 0.03	87 \pm 1
Acrylic Plastic 2 (experiment IV)	0.61 \pm 0.03	0.17 \pm 0.03	72 \pm 6

Table 3. XRF results of tape-lift tests on 4"x 6" samples in both experiments III and IV.

Again, the above table indicates that a significant amount of dust was removed by the water from the surface. In three of the four measurements in Table 3, a significant amount of dust was removed from the surface by the water. The value of 16%, however, is quite low in comparison to the other five results (including those in Tables 1 and 2), which are all in a range from 71% to 87%. We have no experimental justification for excluding this low value. However, because of the uncertainty that it introduces, we decided to repeat the measurement once again. We also introduced changes in the procedure that make the experiment better simulate the actual conditions under which the cavity will be filled; we let the dust stay on the surface for a significantly longer period before wetting it, and we filled and emptied the beakers with water at a much slower rate.

5.0 Experiment V

5.1 Preparation and Procedure

The fifth experiment was performed with two 4"x 6" acrylic plastic samples. Both acrylic plastic samples were rinsed with de-ionized water and dried in a clean room. We blew mine dust on the cleaned samples and let dust settle in the glove-box. Ninety-one hours later we took sample 1 off the hanger and put it into a 2000 mL beaker. We then covered the beaker with plastic wrap to prevent dust entering from outside. We brought them to the clean room and performed tape-lift test with the #369 mylar tape. We first did the tape-lift test on both surfaces of the sample. We used the same tape, repeatedly pressing and lifting it at four different places, trying to get an average distribution because of the non-uniform dust deposition on the acrylic plastic surface. The sample was slowly put back into the beaker. Then, de-ionized water was added into the beaker through a siphon with volume rate of 5.8 mL

per minute until the water covered the sample surface areas to be tested. This fill process took about four hours. Immediately, we used the same siphon to empty the beaker. Figure 5 illustrates the procedure for filling and emptying.

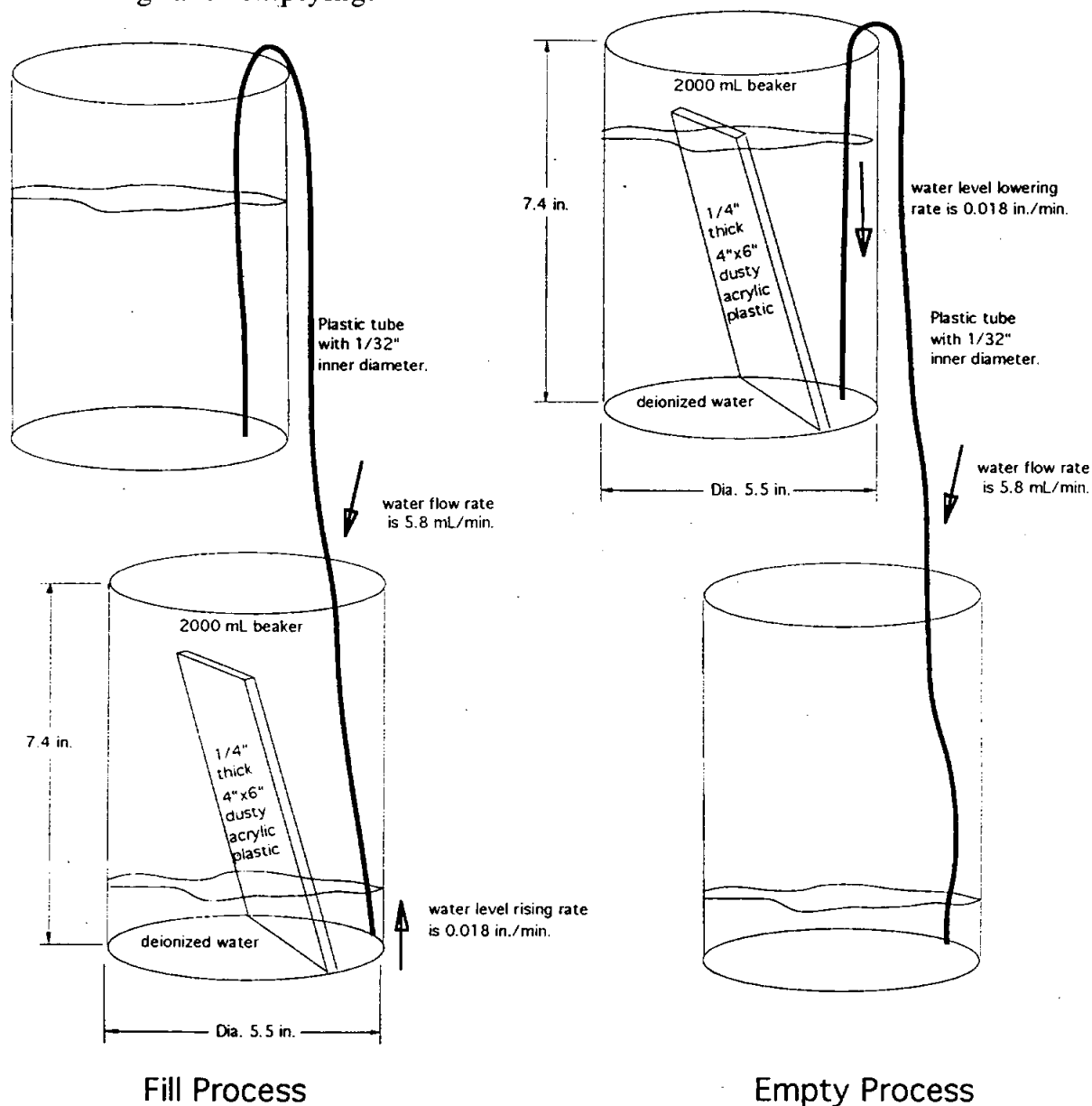


Figure 5. Using a siphon to add and empty the beaker that contains a dusty acrylic plastic sample.

The figure shows that the water level rising rate is 0.018 in/min in our experiment. This rate is close to the anticipated rate in the cavity. After the sample was dry, we did the tape-lift test on both surfaces of the sample, again pressing and lifting a tape at four different (not previously sampled) places on the sample surfaces. All these tapes (including a background tape) were sent for x-ray fluorescence analysis. Sample 2 had stayed in the glove box for 201 hours and was analyzed with the

same procedure as sample 1, except that sample 2 was held vertical instead of slightly inclined in the beaker.

5.2 Results

Table 4 shows the x-ray results of experiment V.

	Dust amount on the #369 Mylar tape ($\mu\text{g}/\text{cm}^2$)		Percentage of dust removed (%)
	Before immersion	After immersion	
Acrylic Plastic 1 (experiment V)	1.48 \pm 0.04	0.16 \pm 0.02	89 \pm 2
Acrylic Plastic 2 (experiment V)	5.40 \pm 0.06	0.125 \pm 0.02	98 \pm ₁ ⁰

Table 4 XRF results of tape-lift tests on 4"x 6" samples in experiment V.

Again, the above table indicates that a significant amount of dust was removed by the water from the surface. Although the water level rising rate is slower than the actual anticipated rate, the amount of dust removed by static water is still maintained around 90%.

6.0 Summary

Results of all five experiments are summarized in Figure 6 as percentage of dust removed by water versus different amounts of dust on acrylic plastic surfaces. If we include all results, the average for the dust removal is 75%, and the standard deviation (δ_n) is 24%. If we exclude the result of 16% (which seems anomalous to us), we obtain a range of values for 70 to 98% and an average of 83% for the percentage (by weight) of mine dust removed from acrylic plastic surface by still water. Then, the standard deviation (δ_n) is 9%. We point out, however, that the actual circumstance in the SNO cavity will be different than these experiments. The dust will have resided longer on the acrylic vessel's surface.

**I would like to thank Dr. Robert Stokstad for his guidance in conducting these experiments and writing this report.

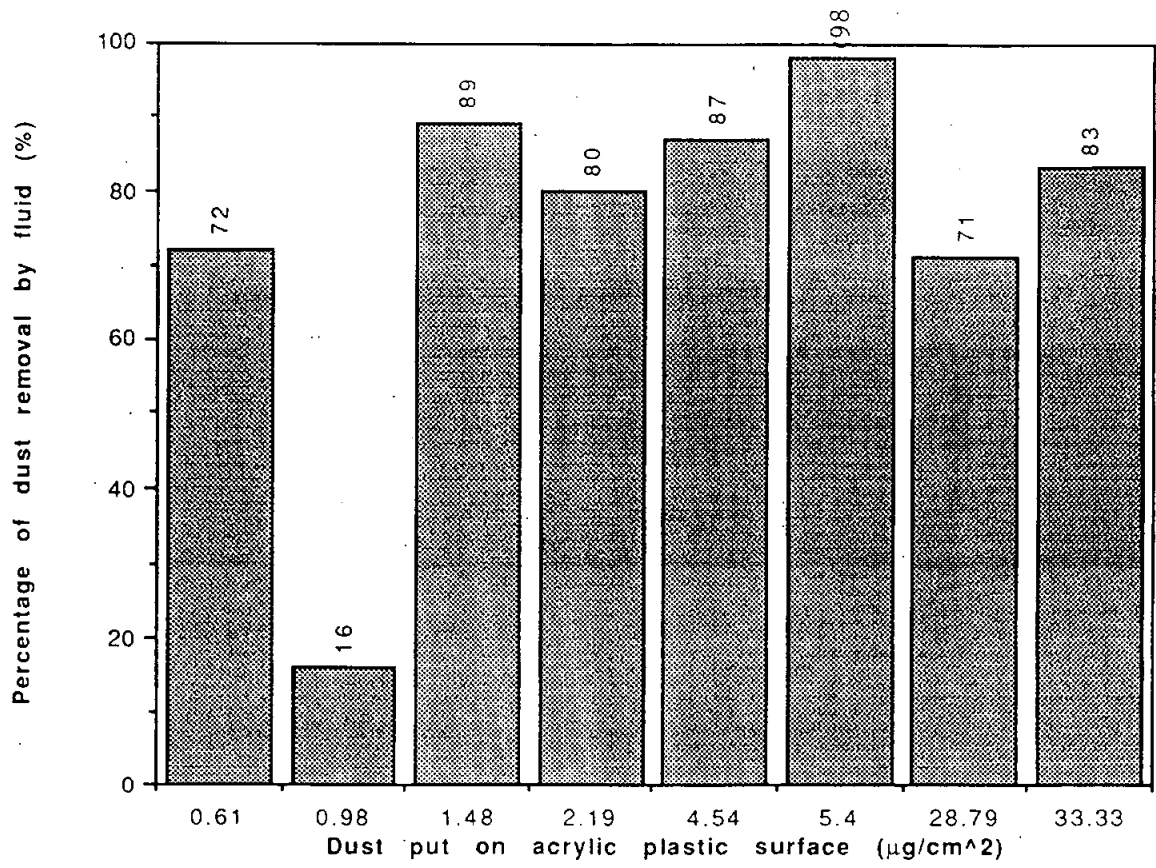
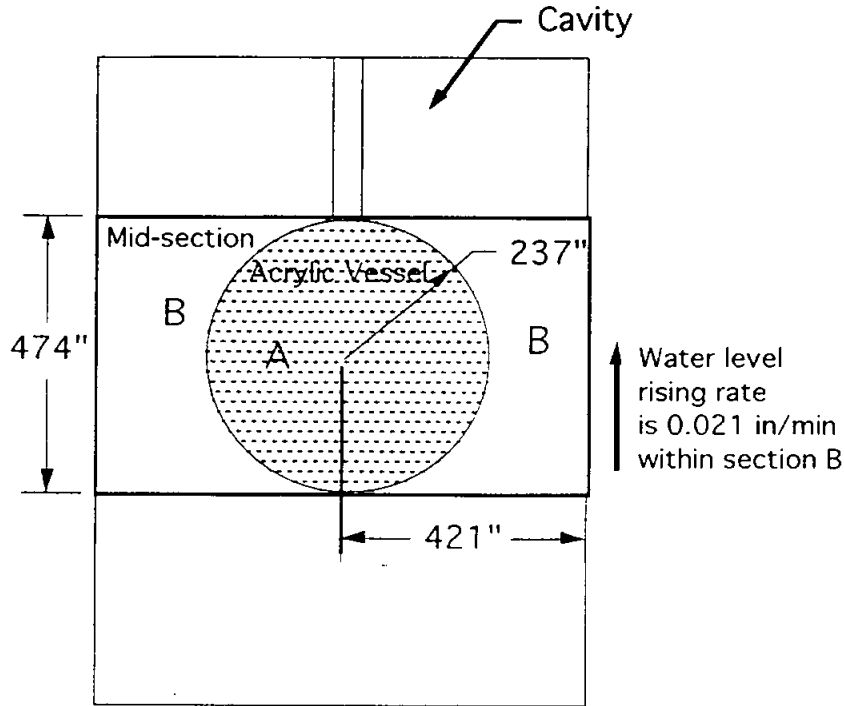


Figure 6. Efficiency of dust removed by water versus different amounts of dust on acrylic plastic surfaces.

Appendix

A simplified calculation of the actual water level rising rate within section B is listed below:

Water flow rate is 150 L/min or 2.5 kg/s



$$\text{Volume A} = \frac{4}{3} * \pi * (237 \text{ in})^3 = 55,761,397 \text{ cubic inches.}$$

$$\begin{aligned} \text{Volume B} &= \pi * (421 \text{ in})^2 * 474 \text{ inches} - \text{Volume A} \\ &= 208,170,820 \text{ cubic inches.} \end{aligned}$$

Since one Liter = 61.02 cubic inches,

$$\text{Volume B} = 3,411,518 \text{ Liters.}$$

$$\begin{aligned} \text{Time required to fill volume B} &= 3,411,518 \text{ Liters} \div 150 \text{ L/min} \\ &= 22,743 \text{ minutes.} \end{aligned}$$

$$\begin{aligned} \text{Therefore, the average water level rising rate within section B} \\ &= 474 \text{ inches} \div 22,743 \text{ minutes} \\ &= \mathbf{0.021 \text{ in/min.}} \end{aligned}$$

^{222}Rn emanation into vacuum

Manqing Liu, H. W. Lee, A. B. McDonald

Department of Physics, Queen's University, Kingston, Ontario, Canada K7L 3N6

August 1992

Abstract

A low-background ZnS scintillator cell based on a design by Lucas has been developed for ^{222}Rn detection. Typical cells have 63% detection efficiency and 3 counts per day background. The cells have been used in measurements of ^{222}Rn emanation rate into vacuum from materials to be used under water in the Sudbury Neutrino Observatory (SNO) solar neutrino detector. The results are presented and the impact on detector design is discussed.

To be submitted to Nucl. Instrum. Meth. Phys. Res.

*How are the
count rates and the
background levels
on the detector being
checked?*

1 Introduction

ZnS-lined scintillator cells (Lucas cells) have been used in radon detection for over 30 years [1, 2]. Most of the development work during this time has been concentrated on increasing detection efficiency. On the other hand, all these cells have relatively high background (several counts per minute). A low background, reasonably high detection efficiency radon detector is required to determine the background caused by radon and its progeny in the Sudbury Neutrino Observatory (SNO), a heavy-water (D_2O) neutrino detector under construction near Sudbury, Ontario, Canada [3]. Figure 1 shows the main parts of the detector. Neutrino interactions in the D_2O produce relativistic electrons or free neutrons. The neutrons are thermalized in the D_2O and are subsequently captured, generating γ -rays which in turn produce relativistic electrons. The electrons from either source will produce Čerenkov photons which pass through the D_2O , through the acrylic vessel which contains the D_2O , through the ultrapure H_2O used as background shielding and to the photomultipliers (PMTs) where they are detected.

The most serious source of background in the SNO detector is the radiation from naturally occurring radionuclides. ^{238}U and ^{232}Th and their daughters (particularly ^{214}Bi and ^{208}Tl) can contribute to the background by high energy β and γ -rays emitted in their decay. Monte Carlo calculations [3] shows that the tolerable concentration of the U chain in secular equilibrium is about 15×10^{-14} gU/ g in the H_2O nearest to the acrylic vessel, and 1×10^{-14} gU/ g in the D_2O .

The emanation of ^{222}Rn and ^{220}Rn and the leaching of their parent radium (^{226}Ra ,

^{224}Ra) from materials into water can cause substantial disequilibrium in the water. The leaching of radium in the SNO detector is being studied by SNO collaborators at Oxford and Queen's [4]. There exists a body of literature on radon emanation from building materials (such as bricks, gypsum board, etc.) which have relatively high radium concentration. Measuring the ^{222}Rn emanation rate from low radioactivity detector materials such as stainless steel, signal cables and PMTs is the objective of the work reported in this paper.

By detecting ^{222}Rn , the rate of 2.45 MeV background gamma rays in the SNO detector from ^{214}Bi decay is determined directly even if there is disequilibrium in the radium or preceding long-lived nuclei. ^{222}Rn has a half-life of 3.8 days, but all daughters before ^{214}Bi have fast half-lives. ^{220}Rn , with a 55 second half-life, is more difficult to detect and requires different techniques [4, 5].

In the first section of this paper, the development of low background scintillation cells is described together with test results. Such cells were used in the measurements of ^{222}Rn emanation into vacuum discussed in the second section. These measurements were also carried out in such a way as to distinguish between ^{222}Rn outgassing and ^{226}Ra -supported radon emanation, which is more important in the SNO detector. In the third section the impact of ^{222}Rn emanation in the SNO detector and some further developments on the scintillation cell is discussed.

2 Development of a low-background scintillation cell

A Lucas cell detector consists of a chamber which is coated on the inside with ZnS

scintillator. An activator such as silver is put into the ZnS to make it scintillate. A photomultiplier is coupled to the window of the cell to detect the light emitted when an alpha particle from the decay of radon or its daughters strikes the ZnS. The cell is filled and sealed through a valve. Typically a SwagelokTM Quick-Connect is used because of its automatic shutoff feature when it is disconnected from the filling apparatus.

In order to have high detection efficiency, a large volume cell is often used [6]. However a larger volume needs more ZnS to coat the surface which results in a higher background. The largest volume with minimum surface area is a spherical design. The main factors considered in a new scintillation cell design are described below:

- 1). Cell body material. The material to be used for the cell body must have a low alpha particle surface-emission rate. Ultraviolet-transmitting (UVT) acrylic is one of the best among low radioactivity materials (< 10 ppt U, Th [4, 7]) and is also transparent. Methylene chloride solvent is used to seal an acrylic window to the cell body and to dissolve the acrylic surface to hold the ZnS coating.

- 2). ZnS sample selection. Six different ZnS (silver activated) scintillator samples were tested for their relative light output and background. About 10 mg/cm² of ZnS was sandwiched between two flat pieces of acrylic sheet, taking care to seal the edges and exclude air. After a three day wait to allow radon from residual air to decay away, a PMT was coupled to one side and the background count rate was determined. The relative light output was determined by comparison of the pulse amplitude spectrum from each sample.

There was about a factor of ten variation in the background rate and a factor of

five variation in light output among the six samples tested. The sample from Johnson Associates (Montville, NJ, USA 07045) was selected as the best compromise between light output and background rate.

3). ZnS thickness optimization. The ZnS thickness has to be optimized for light yield and radioactivity background. The ZnS was coated on a flat piece of acrylic by the following deposition method [8]. First the acrylic piece was submersed in a solution of ZnS suspended in ethyl alcohol. The thickness of the ZnS layer was varied by varying the deposition time. After the acrylic piece was taken out from the solution and dried, methylene chloride was used to fix the ZnS onto the acrylic. The ZnS thickness was obtained by the difference in weight before and after the deposition.

Two different geometries were investigated: "transmission" and "reflection". The pulse height spectra obtained using a ^{241}Am alpha source are shown in Figure 2 (a, b) for these two cases. "Reflection" geometry gives an optimum ZnS thickness of about 10 mg/cm^2 , equal to the range of a 5 MeV alpha particle in ZnS. This thickness was chosen for our cells.

what is spectrum?

4). PMT selection. A low noise PMT is preferred for low background measurements. However the light amplitude from the ZnS scintillator is much higher than the PMT noise amplitude, so the choice of PMT is not critical. Also the scintillation light from ZnS(Ag) peaks is in the blue (4500 \AA) region which matches the response of bi-alkaline PMT photocathodes [9].

X

5). Cell shape. The shape of the Lucas cell was chosen to maximize the light striking

the PMT and minimize the background. A hemispherical cell with a transparent window was designed. The outside diameter of the cell is two inches to match the diameter of the Philips XP2262B PMT chosen. Coating the cell window with a very thin ZnS layer results in high detection efficiency but some of the pulses are degraded into PMT noise. We chose not to coat the cell window, thus sacrificing detector efficiency, but obtaining pulses clearly separated from the PMT noise.

The hemispherical two-inch diameter scintillation cell designed with the above considerations is shown in Figure 3. Figure 4 shows a typical pulse height spectrum with the cell filled with radon. For comparison, Figure 4 also shows a spectrum obtained from a commercial Lucas cell [10] with a cylindrical shape. For the hemispherical design, the signals are very clearly separated from the PMT noise. Furthermore, the cell background was measured to be 3 counts per day for the new hemispherical cell (surface area = 20 cm^2), as compared to 3000 counts per day for the commercial cell (surface area = 145 cm^2). For the commercial cell, the type and thickness of ZnS, the method of ZnS deposition and the radioactivity of the cell body material (in this case aluminum) together give rise to the higher background.

We can rule out several sources which might produce background scintillations in the cell. Cosmic rays do not produce significant scintillation in the thin ZnS, nor do β and γ -rays [11]. Assuming the air has a ^{222}Rn concentration of 2 pCi per liter [12], then our cell with a volume of 12 cm^3 and a residual pressure of 200 microns would have about 6×10^{-2} counts per day. Acrylic even at a 100 ppt U level would give less than 1 count per day

for our cell design. Hence the background of the cell is mainly from natural radioactivity in the ZnS. The alpha counting rate was measured to be about 15 counts per day per gram of ZnS. If we assume all these counts are from the ^{238}U decay chain alphas and the chain is in secular equilibrium, then the inferred U level is about 2×10^{-9} gU/g ZnS (i.e. 2 ppb).

The cell detection efficiency is defined as the measured alpha decay rate divided by the actual Rn decay rate. An efficiency calibration was done by putting a well determined amount of Rn into the hemispherical scintillation cell and counting. The amount of Rn inside the cell was calibrated by Bigu [16]. The detection efficiency was found to be $3 \times (62 \pm 3 \%)$ compared to 66.6% of the geometric area covered with ZnS. The factor of 3 comes from the three alpha decays associated with each ^{222}Rn decay (^{222}Rn , ^{218}Po and ^{214}Bi) when they come to equilibrium about 3 hours after filling the cell.

Additional background identification was done by recording the time associated with each event. For ^{222}Rn , the alpha from its decay is followed by the ^{218}Po ($t_{\frac{1}{2}} = 31$ minute) alpha. The alpha from the decay of ^{220}Rn is followed by the ^{216}Po ($t_{\frac{1}{2}} = 0.14$ second) alpha. For total rates which are low (as in measuring the scintillation cell backgrounds), two events within 0.5 second of each other have a very high probability of being from ^{220}Rn . It is interesting to note for an accumulated background run of 72 hours on 30 mg of ZnS, we did not observe any ^{220}Rn decays, which indicates there is the equivalent of less than 5 ppb ^{232}Th in the ZnS.

3 ^{222}Rn emanation measurements

$$\bar{n} = 1 - (1 - p)^n \quad 7$$

In materials, ^{226}Ra can occur in the grains, crystals, etc, making up the materials. When ^{226}Ra decays, some of the ^{222}Rn generated close to the surface of the grains can escape into the space between the grains by virtue of their recoil energy. ^{222}Rn trapped deeper inside grains and crystals can escape by diffusing out (outgassing). Only a fraction of the ^{222}Rn created by the decay of radium is given off to the outside; the remainder of the radon undergoes decay in the material. We describe a system and a procedure used to measure the rate at which ^{222}Rn is emanated by a material into vacuum.

The radon emanation system consists of the ^{222}Rn emanation chamber, ^{222}Rn transfer apparatus (" radon board ") and hemispherical scintillation cell as shown in Figure 5. The radon emanation chamber is a cylindrical acrylic chamber 30 cm outer diameter and 65 cm long. Its wall thickness is 12 mm, and the ends are sealed with Viton O-rings. The purpose of the radon board is to extract radon from a mixture of gases (O_2 , N_2) with lower freezing points and then transfer it into a scintillation cell. Its design is based on the one used by Key et al [13] in studies of radium distribution in oceans. All the parts of the radon board are made of stainless steel SwagelokTM fittings. Brass wool was put into the traps to increase the ^{222}Rn trapping efficiency.

The radon collection efficiency of the system was calibrated by putting ^{222}Rn from a calibrated source into the emanation chamber, extracting the ^{222}Rn using the " radon board " and then putting it into the scintillation cell. The total efficiency is defined as the ratio of the counting rate of the scintillation cell after the extraction to the amount of ^{222}Rn put into the emanation chamber. A $(33 \pm 5 \%) \times 3$ total efficiency was obtained,

which includes 72 ± 5 % efficiency for pumping the radon out of the emanation chamber into the large trap, a 75 ± 5 % efficiency for transferring the radon from the large LN₂ trap to the small trap and then into the scintillation cell and $(62 \pm 3 \%) \times 3$ efficiency for detecting a ²²²Rn decay in the cell. The factor of 3 in the efficiency arises from the three alpha particles emitted in the decay of ²²²Rn and its daughters.

The background of the system was measured with no material placed inside the acrylic emanation chamber. Contributions to the background come from the acrylic chamber, the radon board and the scintillation cell. The lowest background achieved for the whole system was measured to be about 20 counts per day (where 12 counts per day were from the chamber, 5 from the radon board and 3 from the scintillation cell). It was found that the background rate in the chamber was higher shortly after large amounts of radon were emanated into the chamber by radioactive samples. The higher rate decreased with time at a rate consistent with the hypothesis that it comes from adsorption of ²²²Rn on the walls of the chamber. The scintillation cell background increases by 1 count a day for every 10^4 ²²²Rn decays in the cell because of the 22 year ²¹⁰Pb.

The measurements of radon emanation from materials were performed in the following way. The material for which the ²²²Rn emanation was to be measured was put inside the emanation chamber and pumped for more than a day. Typically the chamber reached a vacuum of 200 - 500 microns. Then the chamber was sealed in order for the ²²²Rn to emanate. After a time t_a , the ²²²Rn in the chamber was extracted and transferred to a scintillation cell. After a 3 hour wait for ²²²Rn to come to equilibrium, the number

(All counted and sealed again?)

of counts N_a was obtained for 20 hours of counting. The chamber was sealed and the procedure was repeated for emanation times $t_b, t_c, \text{ etc.}$ over about 10 days total. By plotting $N_i/(1-e^{-\lambda t_i})$ as a function of the cumulative time, it is possible to distinguish outgassing of absorbed radon from Ra-supported Rn emanation. For ^{226}Ra -supported ^{222}Rn emanation, the function would be a constant value. Contributions from outgassing of absorbed radon produce excess counts for times less than about 4 days. If radon emanation from ^{226}Ra decay was clearly observed, an average value for emanation times much greater than 4 days was determined, together with an uncertainty. In situations with low statistics or without an observable steady emanation rate, only an upper limit for Ra-supported ^{222}Rn emanation could be determined.

The experimental results are summarized in Table 1. In most circumstances, only an upper limit for the ^{222}Rn emanation rate was obtained. As an example of the results, Figure 6 shows the time evolution of the emanated ^{222}Rn for the high-density polyethylene cable. There is some outgassing of absorbed radon initially and after several days all the ^{222}Rn is supported by ^{226}Ra decay in the cable.

A ^{222}Rn emanation rate can be calculated by assuming that it recoils directly out from an ideal smooth surface because of its kinetic energy. This calculated ^{222}Rn emanation rate for known recoil ranges and bulk radioactivity is about 1000 times lower than the observed Ra-supported ^{222}Rn emanation rates. This suggests that ^{222}Rn is diffusing out from the decay of ^{226}Ra contaminants deeper within the material.

4 Impact on the SNO detector design

The ^{222}Rn emanation rates of the major components of the SNO detector have been measured. If the ^{222}Rn emanation rate into water is similar to that into vacuum, then the total ^{222}Rn emanated from submersed materials in the water can be calculated.

The H_2O is divided into an "inner" volume (1700 tonnes) between the PMT support structure and the acrylic vessel and an "outer" volume (5500 tonnes) between the PMT support structure and the cavity liner. A 99% water-tight seal on the PMT support structure reduces mixing of H_2O in the outer region with the more critical low-radioactivity H_2O inside. There will not be a significant amount of emanated radon in the D_2O because there is very little material other than clean acrylic in contact with it. The ^{222}Rn emanated from the submersed materials in the two volumes of H_2O are presented in Table 2. The last column (supported radon from material emanation) is given by the product of the area or length, the emanation rate and the mean life of ^{222}Rn (3.8 day/ $\ln 2$).

During the assembly of the detector, some mine dust will be deposited on the surfaces, in spite of extreme care with cleanliness. The final cleanup is expected to reach a level of $0.4 \mu\text{g}$ dust per cm^2 inside the PMT support structure [4] which gives a total of 23 grams of dust over the 5673 m^2 . The dust outside the PMT support structure will be harder to clean up because the surfaces have many hidden crevices. There we are aiming for $4 \mu\text{g}$ of dust per cm^2 which over the 6400 m^2 gives 256 grams of dust.

The total emanated radon in Table 2 can be compared to the design objective for the SNO detector. The 1700 tonnes of H_2O inside the PMT support structure is expected to contain less than $15.0 \times 10^{-14} \text{ gU/g}$ (which supports 1.5×10^6 radon) and the 5300

tonnes of H₂O outside the PMT support structure should contain less than 45.0×10^{-14} gU/g (which supports at least 4.5×10^6 radon). As shown in Table 2, the emanated radon load outside the PMT support structure could be higher than the emanated radon load inside the structure. The H₂O water recirculation system will take water from the outer region, put it through ion exchange resins, high efficiency vacuum degassing and ultraviolet radiation before returning it to the critical inner H₂O volume.

Two other sources of radon are the plastic cavity liner and the cover gas above the H₂O and D₂O surfaces. The design goal for the cavity liner is to have no more than 2 ²²²Rn m⁻²hr⁻¹ penetrating through the liner into the water. Independent measurements indicate that the design goal can be met [16]. If the cover gas is constrained to contain less than 2×10^{-4} pCi/liter of radon, then the exchange of radon into the water will not be a significant problem [14].

5 Further development on scintillation cells

The transfer efficiency can be improved by immersing the scintillation cell into liquid nitrogen while the Rn is being transferred. One effect of doing this is an effective increase of the pressure in the cell by a factor of four due to the lower temperature. The other effect is that the inner surface of the cell becomes a cryogenic pump for radon.

We have developed several cell designs which survive repeated submersion in liquid nitrogen. With this apparatus, nearly all of the Rn collected in the primary ²²²Rn trap can be transferred into the cell. We are continuing to work on the reliability of the cell design as some have developed cracks in the window to body seal.

6 Conclusion

A low background, high efficiency scintillation cell has been developed for Rn detection for the SNO detector. If the ^{222}Rn emanation rate into water is similar to that into vacuum, then the total Rn emanated into the SNO detector is less than the design objectives.

Acknowledgements

We are grateful to Dr. J. Bigu (CANMET, Elliot Lake, Canada) for his assistance in the efficiency calibration of the hemispherical scintillation cell. We also wish to thank G. Mathieu at Lamont-Doherty Geological Observatory (Palisades, NY) for supplying samples of ZnS and Drs. P. Jagam and J. Simpson (University of Guelph) for measurements of U and Th content in materials.

References:

1. H. F. Lucas, Rev. Sci. Instrum. 28, 680 (1957)
2. Andreas C. George, IEEE Trans. Nucl. Sci. 37, 892 (1990)
3. G. T. Ewan et al, Sudbury Neutrino Observatory (SNO) Proposal, SNO-87-12 (1987), and SNO Scientific and Technical Description of Mark II detector, edited by E. Beier and D. Sinclair (1989), see also G. T. Ewan, Nucl. Instrum. Meth. Phys. Res. A314, 373 (1992)
4. C. E. Waltham, E. D. Hallman, P. Doe, R. G. H. Robertson, W. Frati, R. V. Berg, K. T. Lesko, B. C. Robertson and J. J. Simpson, Physics in Canada 48, 135 (1992).
5. B. Sur, H. Lee, X. Zhu, M. Q. Liu and A. B. McDonald, Bull. Amer. Phys. Soc. 37, 1020 (1992)
6. B. L. Cohen, M. Elgayni and B. Duchemin, Nucl. Instrum. Meth. Phys. Res. A286, 594 (1990)
7. J. J. Simpson and P. Jagam, University of Guelph, Canada, private communication.
E. D. Earle, E. Bonvin, G. M. Milton, Chalk River Laboratories, private communication.
8. Manqing Liu, M.Sc thesis, Dept. of Physics, Queen's University, Kingston, Canada (1991)
9. T. Hase, T. Kano, E. Nakazawa and H. Yamamoto, Adv. in Elect. and Electron Phys. 79, 271 (1990)

10. Pylon Electronic Development Company Ltd., Ottawa, Ontario (Canada)
11. R. Kouzes, Princeton University, Private communication
12. *Radon and its Decay Product in Indoor Air*, William W. Nazaroff and Anthony U. Nero, Jr, edit., John Wiley & Sons, (1988)
13. R. M. Key, R. L. Brewer, J. H. Stockwell, N. L. Guinasso and D. R. Schink, *Mar. Chem.* 7, 251 (1979)
14. B. Sur, Sudbury Neutrino Observatory report, SNO-STR-91-055 (1991)
15. X. Zhu, Queen's University at Kingston, Canada, private communication
16. J. Bigu, CANMET, Elliot Lake, Canada, private communication

Table 1 Experimental Rn emanation rates into vacuum

Materials	^{222}Rn emanation rate hour $^{-1}$	^{238}U content [7] 10 $^{-9}$ g/g (ppb)
Molecular sieve 13X	1200 \pm 120 l $^{-1}$	225 \pm 19
Activated charcoal	250 \pm 50 l $^{-1}$	
Silica Gel	440 \pm 50 l $^{-1}$	197
Coax cable RG-59	60 \pm 30 m $^{-1}$	
Twinaxial PE cable	<2 m $^{-1}$	
Coax cable 8240	6 \pm 2 m $^{-1}$	
Coax cable 9067	<0.6 m $^{-1}$	< 10
Kevlar 3/8" rope	<0.3 m $^{-1}$	0.07
8" PMT	<20 PMT $^{-1}$	
Low-rad. glass	<1.6 m $^{-2}$	50
Aluminum reflector	<1.5 m $^{-2}$	
Black ABS plastic	<1.1 m $^{-2}$	20 \pm 5
White PE	<0.9 m $^{-2}$	
Acrylic	<0.1 m $^{-2}$	
Al plates	<0.5 m $^{-2}$	5
SS 304L [G.Graves]	<15 m $^{-2}$	<1
SS 304L [Sandvik]	<0.3 m $^{-2}$	

Table 2. Rn emanation in the SNO detector

Between the PMT support structure and the acrylic vessel

Material	Quantity	^{222}Rn Emanation rate	Supported ^{222}Rn
Acrylic vessel	452 m ²	<0.1 m ⁻² hr ⁻¹	<6 × 10 ³
Suspension rope	180 m	<0.3 m ⁻¹ hr ⁻¹	<7 × 10 ³
PMT glass	473 m ²	<1.6 m ⁻² hr ⁻¹	<1 × 10 ⁵
Al Reflectors	673 m ²	<1.5 m ⁻² hr ⁻¹	<1 × 10 ⁵
ABS in PMT support	3665 m ²	<1.1 m ⁻² hr ⁻¹	<5 × 10 ⁵
Stainless Steel	410 m ²	<0.3 m ⁻² hr ⁻¹	<2 × 10 ⁴
Mine Dust (0.4μg/cm ²)	23 g	44 g ⁻¹ hr ⁻¹ [15]	1.3 × 10 ⁵
Total			<9 × 10 ⁵

Outside the PMT support structure

Material	Quantity	²²² Rn Emanation rate	Supported ²²² Rn
Stainless Steel	650 m ²	<0.3 m ⁻² hr ⁻¹	<3 × 10 ⁴
Coax cables (a)	190,000 m	<0.6 m ⁻¹ hr ⁻¹	<1 × 10 ⁷
Plastic liner	2000 m ²	2 m ⁻² hr ⁻¹ (b)	5.3 × 10 ⁵
ABS in PMT support	1250 m ²	<1.1 m ⁻² hr ⁻¹	<2 × 10 ⁵
Dust (4μg/cm ²)	256 g	44 g ⁻¹ hr ⁻¹ [15]	1.5 × 10 ⁶
Total			< 1 × 10 ⁷

(a) The coax cables will be bundled and the exposed area is estimated to be 2500 m².

(b) Design goal.

Figure Captures:

Fig. 1 Outline of the proposed SNO detector. The detector would be located at a depth of 6800 feet in INCO's Creighton mine near Sudbury, Ontario, Canada.

Fig. 2. Pulse height spectra for different ZnS thicknesses under (a) " transmission " geometry and (b) " reflection " geometry.

Fig. 3 Diagram of a 2 inch diameter hemispherical scintillation cell.

Fig. 4 Pulse height spectrum measured for our cell. The spectrum measured with a commercial cell is also shown.

Fig. 5 Diagram of radon emanation measurement system. The Rn was first trapped in the liquid nitrogen cooled primary trap. Then the primary trap is warmed and the radon was transferred to the smaller trap immersed in liquid nitrogen. Finally the small trap was warmed and the radon was filled into the scintillation cell by free expansion.

Fig. 6 Rn emanation measurement results from Belden high density polyethylene twincoaxial cable [• — before decay correction, Δ — after decay correction, $N_i/(1-e^{-\lambda t_i})$]. The horizontal axis represents the day which the chamber was opened, radon was extracted from the emanation chamber and resealed. It can be seen that the corrected emanation rates are nearly constant after a couple of days, indicating that the Rn is supported by Ra decay.

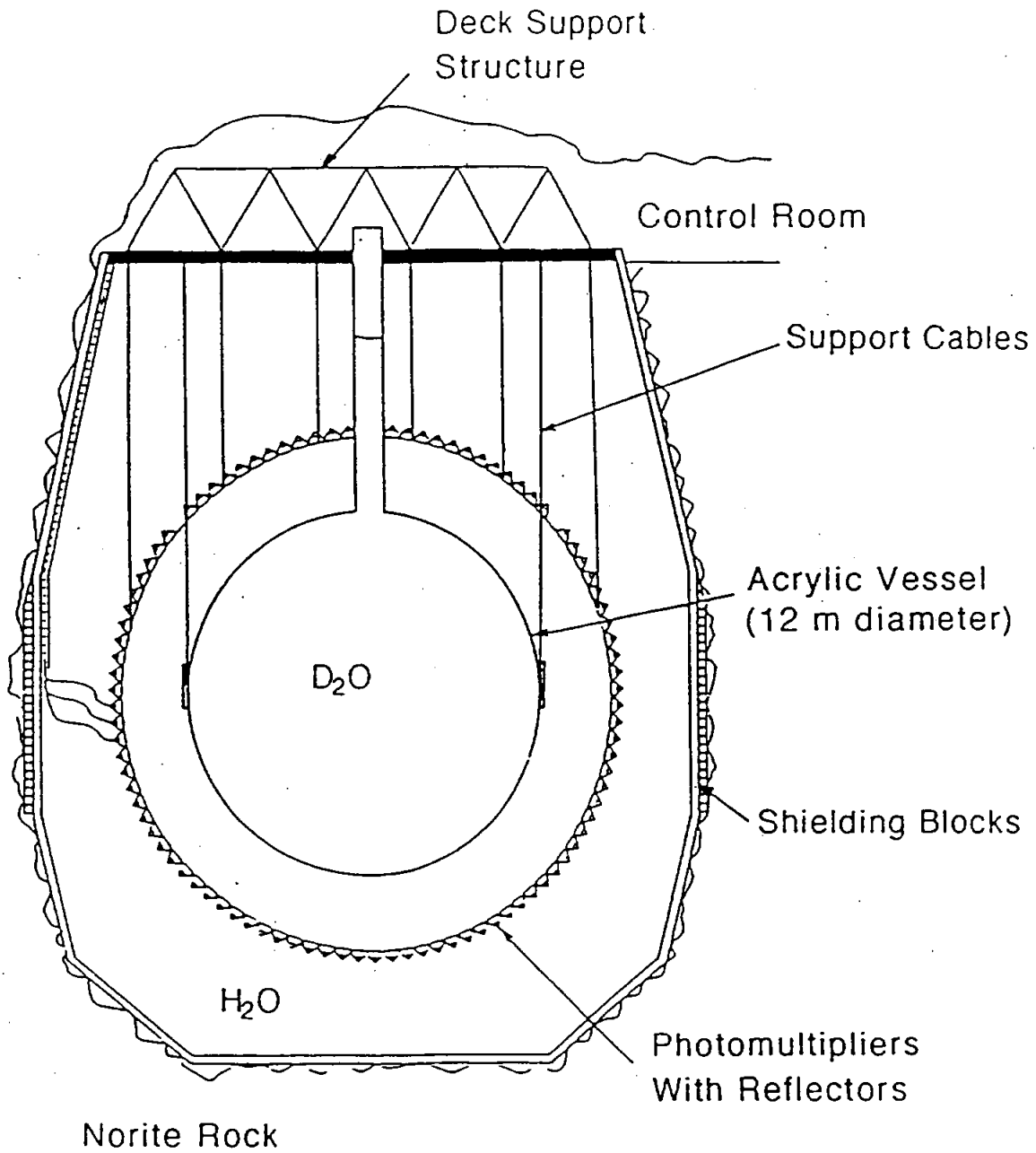


Figure 1 A cross section drawing of the SNO Neutrino Detector

Figure 2 (a)

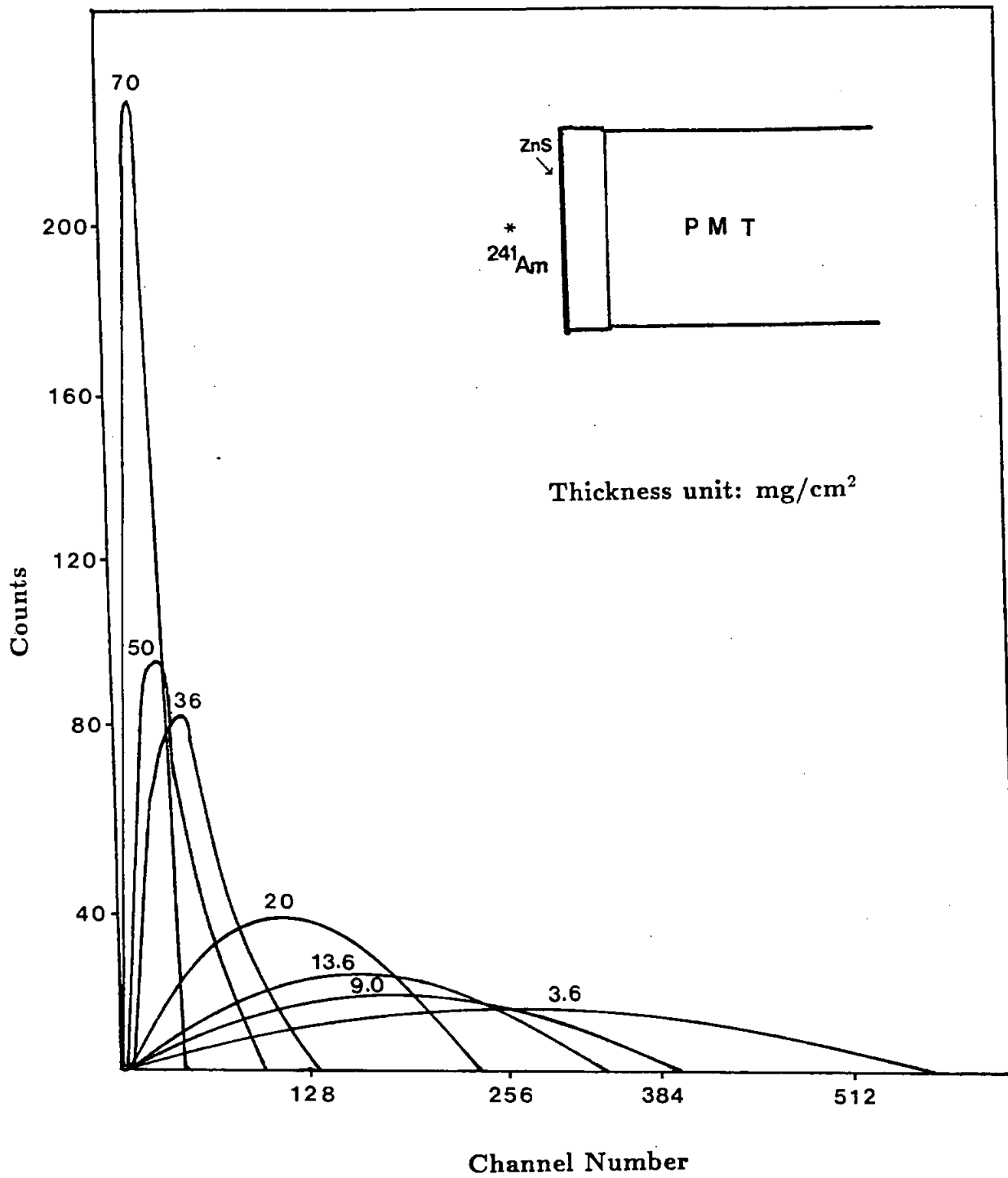


Figure 2 (b)

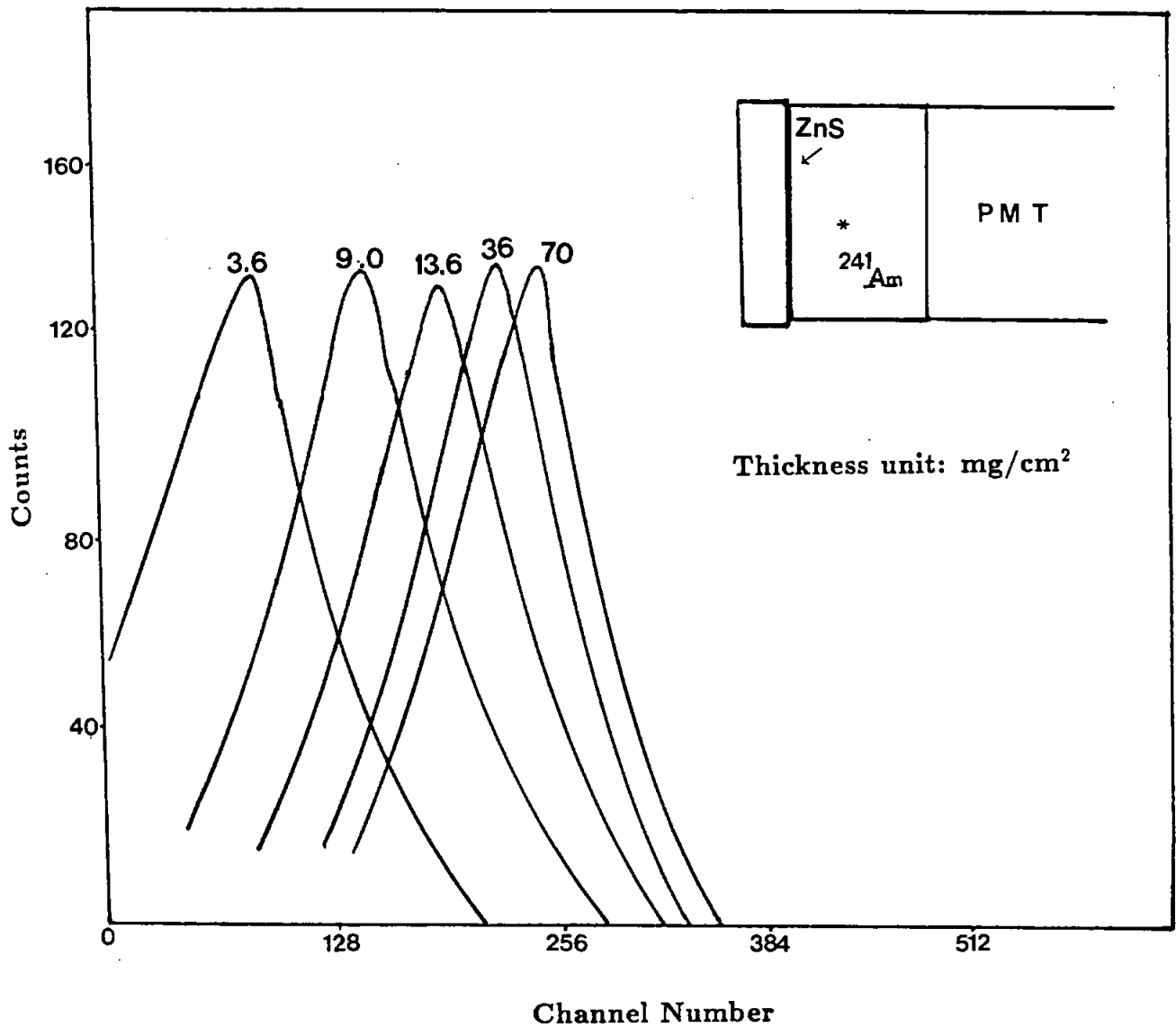


Figure 3.

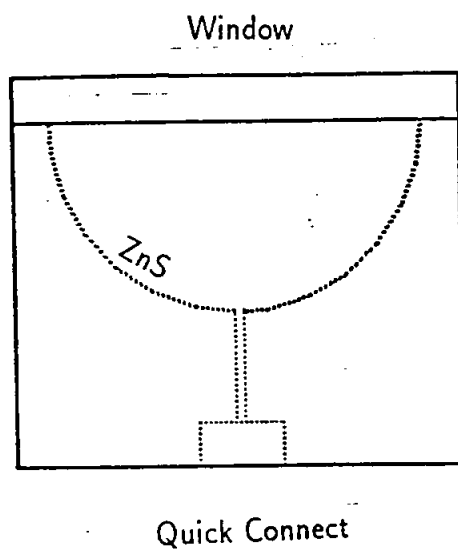
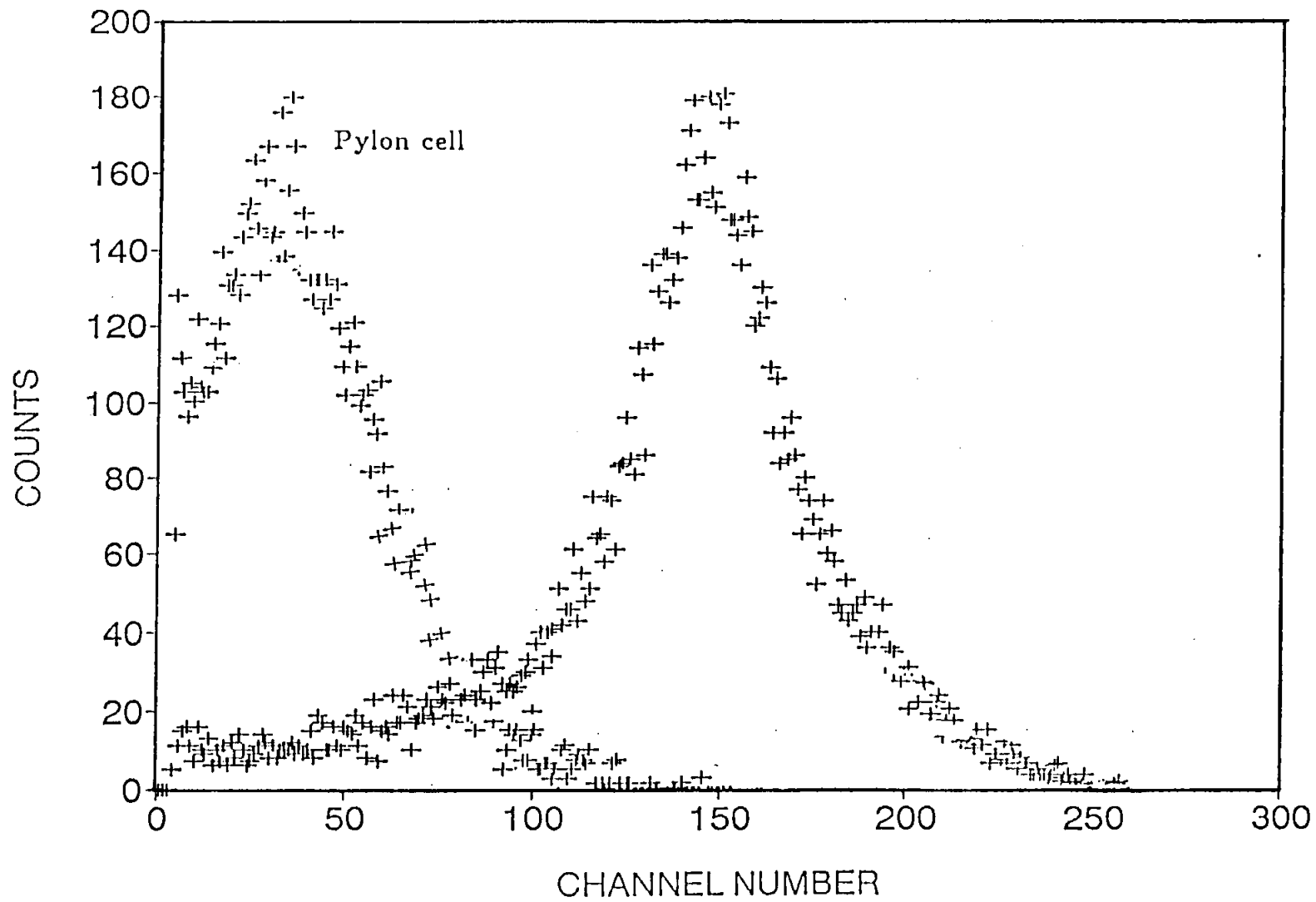


Figure 4



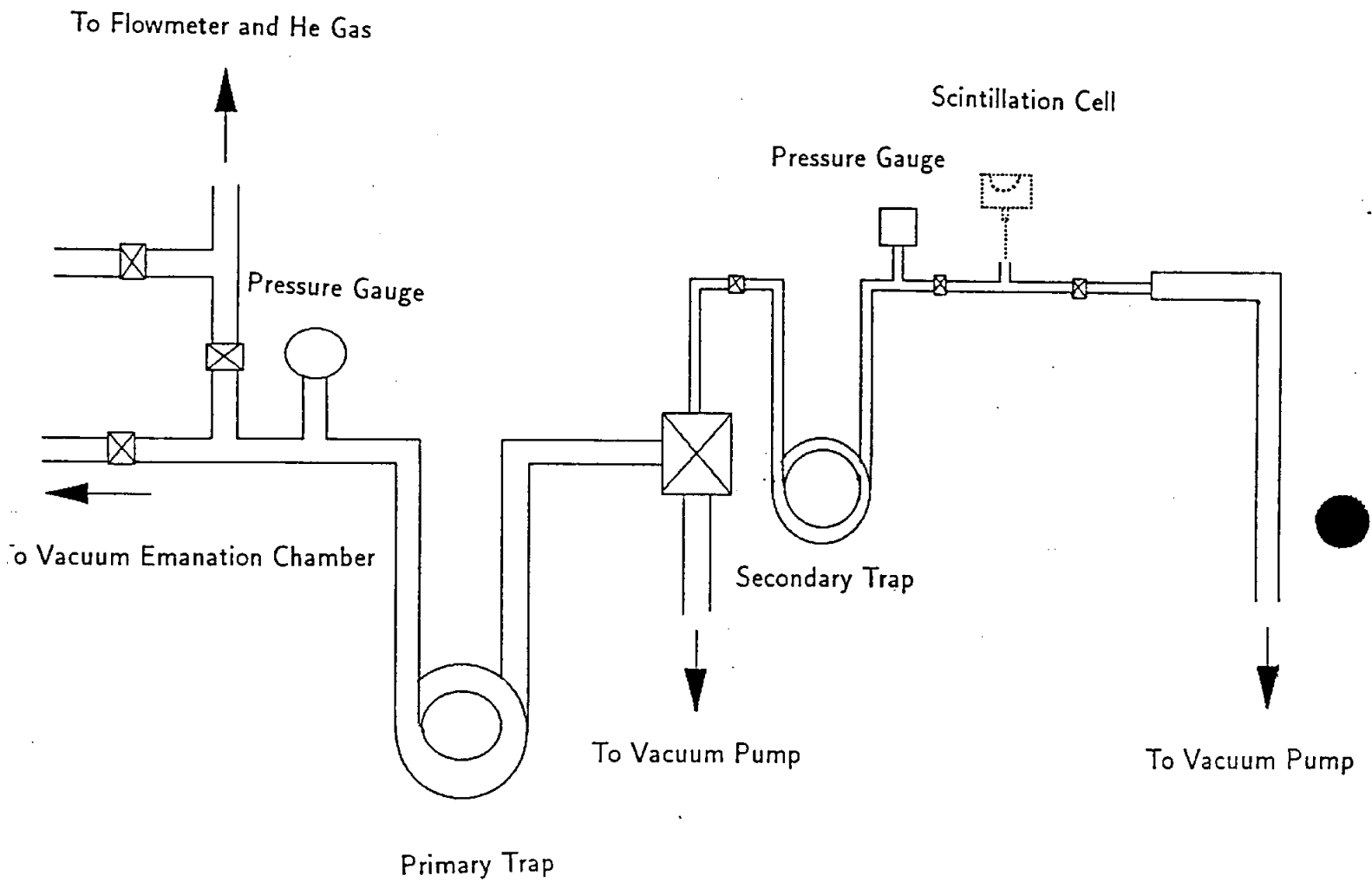


Figure. 5

Figure 6

